The Astrophysical Journal, 980:56 (10pp), 2025 February 10 https://doi.org/10.3847/1538-4357/ada5fd

Sporadic Dips from Extended Debris Transiting the Metal-rich White Dwarf SBSS 1232+563

J. J. Hermes[1], Joseph A. Guidry[1,6], Zachary P. Vanderbosch[2], Mariona Badenas-Agusti[3], Siyi Xu (许偲艺)[4], Malia L. Kao[5], Antonio C. Rodriguez[2], and Keith Hawkins[5]
[1] Department of Astronomy,Boston University, 725 Commonwealth Avenue, Boston, MA 02215, USA; jjhermes@bu.edu
[2] Division of Physics, Mathematics, and Astronomy, California Institute of Technology, Pasadena, CA 91125, USA
[3] Institute of Astronomy, University of Cambridge, Madingley Road, Cambridge CB3 0HA, UK
[4] Gemini Observatory/NSF's NOIRLab, 670 N. A'ohoku Place, Hilo, HI 96720, USA
[5] Department of Astronomy, University of Texas at Austin, 2515 Speedway, Austin, TX 78712, USA
Received 2024 November 11; revised 2025 January 2; accepted 2025 January 2; published 2025 February 4

Abstract

We present the discovery of deep but sporadic transits in the flux of SBSS 1232+563, a metal-rich white dwarf polluted by disrupted exoplanetary debris. Nearly 25 yr of photometry from multiple sky surveys reveal evidence of occasional dimming of the white dwarf, most notably evident in an 8 month long event in 2023 that caused a >40% drop in flux from the star. In-transit follow-up shows additional short-timescale (minutes- to hours-long) dimming events. Transiting Exoplanet Survey Satellite photometry suggests a coherent 14.842 hr signal that could represent the dominant orbital period of debris. Six low-resolution spectra collected at various transit depths over two decades show no evidence of significant changes in the observed elemental abundances. SBSS 1232+563 demonstrates that debris transits around white dwarfs can be sporadic, with many years of inactivity before large-amplitude dimming events.

Unified Astronomy Thesaurus concepts: White dwarf stars (1799); Transits (1711); Debris disks (363); Variable stars (1761)

1. Introduction

Although short-period exoplanets are expected to be engulfed as their host star evolves off the main sequence, distant orbiting planets (e.g., beyond Mars in our solar system) are expected to persist all the way to the white dwarf stage (K. P. Schröder & R. C. Smith 2008). Surviving planets provide the gravitational impetus to scatter asteroids and planetesimals onto star-grazing orbits, where we observe the consequence of tidal shredding of these rocks by the central white dwarf. Disrupted material can form dusty disks detectable as an IR excess, as well as gaseous disks with atomic lines detected in emission or absorption, and the material eventually works its way onto the white dwarf, polluting its surface; see the reviews by D. Veras (2016) and J. Farihi (2016).

The prevailing view of accretion of disrupted exoplanetary material onto the photosphere of metal-rich white dwarfs was corroborated by the discovery of deep, irregular transits from rocky debris toward the metal-rich white dwarf WD 1145+017 recurring roughly every 4.5 hr, close to the period expected for a circular orbit near the tidal disruption radius (A. Vanderburg et al. 2015). Several additional metal-rich white dwarfs that exhibit photometric transits have been discovered from transient surveys such as the Zwicky Transient Facility (ZTF), including both long-period transiting systems with dip recurrence timescales greater than 100 days (Z. Vanderbosch et al. 2020; J. A. Guidry et al. 2021), as well as shorter-period systems with recurrence timescales less than 12 hr (Z. P. Vanderbosch et al. 2021).

Patterns in the debris transiting white dwarfs have so far been characterized by reproducibility over a few orbital cycles but wholesale changes over tens of orbital cycles, likely revealing the dynamics around these chaotic circumstellar environments. For example, drifting fragments from one 25 hr orbit to the next are seen in the transiting white dwarf WD 1054-226 (J. Farihi et al. 2022). Long-term changes are also frequently observed in these transiting systems. In fact, WD 1145+017 has seen a drastic reduction in transit activity since roughly 2022 (A. Aungwerojwit & V. S. Dhillon 2024).

One previously claimed candidate transiting debris system is the metal-rich white dwarf SBSS 1232+563. Not to be confused with the Sloan Digital Sky Survey (SDSS), SBSS 1232+563 was first cataloged as a Second Byurakan Survey Star (SBSS), a program initiated in 1974 from the Byurakan Observatory in Armenia to search for galaxies, quasars, and other ultraviolet-bright objects (M. D. Bicay et al. 2000). SBSS 1232+563 was first spectroscopically classified as a DBAZ by D. J. Eisenstein et al. (2006) from an early SDSS Data Release 4 (DR4) spectrum; the classification implies a helium-dominated (DB) spectrum with large contributions from hydrogen (A) and metals (Z[7]). An analysis of the SDSS spectrum along with the photometry plus the Gaia Data Release 2 (DR2) parallax by S. Coutu et al. (2019) find $T_{\rm eff} = 11{,}790 \pm 420$ K, $\log g = 8.30 \pm 0.06$, $\log({\rm H/He}) = -5.52 \pm 0.14$, and $\log({\rm Ca/He}) = -7.41 \pm 0.06$, atmospheric parameters we adopt throughout this work.

Higher-resolution spectroscopy from Keck reveal eight heavy elements (O, Mn, Cr, Si, Fe, Mg, Ca, and Ti) in addition to H and He in SBSS 1232+563, corresponding to a total accretion rate of material in excess of 5×10^9 g s^{-1} (S. Xu et al. 2019). More than 60% of the accreted material is O by mass, which implies that the majority of O delivered was not locked up in rocks such as MgO or SiO_2 (B. Klein et al. 2010).

[6] NSF Graduate Research Fellow.

[7] More recent references classify SBSS 1232+563 as a DZBA given that metals are the dominant spectral component. Historically, this judgment has been done by visual inspection and is therefore somewhat subjective.

An oxygen excess can be interpreted as evidence of water-rich asteroid debris (e.g., J. Farihi et al. 2013; R. Raddi et al. 2015). While the O excess in SBSS 1232+563 appears robust (M. G. Brouwers et al. 2023), there is not enough H measured in the star for H_2O to be responsible for even 20% of this O excess, making the source of excess O an open question (S. Xu et al. 2019).

The IR photometry from Wide-field Infrared Survey Explorer (WISE) does not appear to follow the spectral energy distribution of a single white dwarf; the IR excess at the W1 (3.4 μm) and W2 (4.5 μm) bands was used by J. H. Debes et al. (2011) to argue that SBSS 1232+563 is an excellent candidate to host a dusty debris disk. For a time it was claimed to be the most massive white dwarf with a disk (S. D. Barber et al. 2014), but that analysis used an incorrect mass determination from D. J. Eisenstein et al. (2006); the mass of SBSS 1232 +563 has been refined to a lower value of $0.77 \pm 0.04\,M_{\odot}$ (S. Coutu et al. 2019). Spitzer imaging confirms that the IR excess is real, arising from dusty debris (A. Swan et al. 2020). The Spitzer data also revealed 8% (5σ) variability at 4.5 μm, further evidence that the IR excess is from a debris disk (e.g., J. A. Guidry et al. 2024).

Transits from planetary debris were first suspected in SBSS 1232+563 based on its anomalously large photometric uncertainties in Gaia DR2 (J. Hermes et al. 2018). More detailed variability analysis also incorporating ZTF photometry made SBSS 1232+563 a candidate for transiting debris, although more than 36 hr of high-speed photometry from McDonald Observatory did not reveal any dramatic (>7% depth) dimming events (J. A. Guidry et al. 2021).

Interestingly, fits for the atmospheric parameters of SBSS 1232+563 in S. Coutu et al. (2019) were complicated by the variable photometry, who noted "The SDSS magnitudes for this object are ∼0.3 mag fainter than Pan-STARRS and Gaia, which leads to two different possible solutions. We could not reach a conclusion regarding this discrepancy..." We propose here the solution: SBSS 1232+563 undergoes sporadic and occasionally deep transits from orbiting debris.

In Section 2 we detail the long-baseline survey photometry that shows sporadic dips from planetary debris transiting SBSS 1232+563. In Section 3 we detail more than 37.5 hr of high-speed photometry collected to look for short-period transit events from the source, as well as six sectors of Transiting Exoplanet Survey Satellite (TESS) observations. In Section 4 we put low-resolution spectroscopy collected on SBSS 1232 +563 over many years into the context of the observed transits. We conclude with a discussion in Section 5.

2. Survey Photometry of SBSS 1232+563

Figure 1 shows the full 25 yr photometric baseline collected on SBSS 1232+563. We detail the median magnitudes in each filter used for the relative photometry in Table 1. We further detail the survey photometry we have used, roughly in reverse chronological order in the following.

ZTF. The bulk of our photometry comes from ZTF partnership surveys (F. J. Masci et al. 2019), which we extracted through forced point-spread function (PSF) photometry (see the ZTF Forced Photometry Service (ZFPS) documentation[8]) on the Gaia-measured centroid, yielding 1573 epochs from 2018 March through 2024 May across the ZTF g and r bands. We do not include the ZTF i-band light curve in our analysis due to a lack of epochs, most of which are concentrated years before the 2023 transit. We curate our photometry following the standard recommendations from the ZFPS documentation: we select only `infobitssci` $= 0$ measurements with a signal-to-noise ratio (S/N) > 5 and those brighter than the estimated limiting magnitude inflated by 0.5 mag and do not perform other filtering on the light curves (see J. A. Guidry et al. 2021). We calibrate the measured zero-point magnitudes from the difference imaging to absolute magnitudes and perform color corrections to the cataloged Pan-STARRS 1 (PS1) magnitudes. We finally convert these color-corrected magnitudes to relative fluxes by normalizing the measurements to the median ZTF magnitude and propagating the associated errors. We carried out this procedure for every other survey to do our analysis in relative flux space. ZTF epochs are not corrected for proper motion, sufficient for this 6 yr baseline.

Asteroid Terrestrial-impact Last Alert System (ATLAS). Significant recent photometry comes from ATLAS, which is a system of four telescopes in Hawaii, Chile, and South Africa that scan the sky for moving objects, in the process producing large archives of photometry down to roughly $G < 19$ mag (J. L. Tonry et al. 2018). We do forced photometry on the ATLAS reduced science images[9] using the Gaia-measured centroid of SBSS 1232+563, taking into account the measured proper motion. We apply barycentric corrections to all time stamps due to the multisite nature of ATLAS. Keeping measurements only with S/N > 3, we bin the extracted cyan (c-band) and orange (o-band) photometry to within 1 day, to further boost signal. After binning, we convert all remaining magnitudes to fluxes using the median magnitude of the binned light curve. We retain 669 epochs from 2015 December through 2024 August.

Gaia. For every object classified as a variable by a machine learning algorithm trained on constant objects, Gaia Data Release 3 (DR3) provided multiepoch light curves (L. Eyer et al. 2023). Each individual epoch is observed through one of the Gaia G, G_{RP}, or G_{BP} bandpasses. More than 1300 high-confidence white dwarfs were flagged in Gaia DR3 as variables (M. Steen et al. 2024), including SBSS 1232+563 (Gaia DR3 1571584539980588544). We accessed the epoch photometry of SBSS 1232+563 via `astroquery` (A. Ginsburg et al. 2019), yielding 58 G-band epochs sampled between 2014 September to 2017 April. We only assess the G-band photometry here, as it has more precision and the G_{RP} and G_{BP} span the same observing baseline. The median Gaia magnitude in Table 1 is reported in Vega magnitudes; all other surveys use the AB system.

PS1. We acquired PS1 (K. C. Chambers et al. 2016) DR2 light-curve photometry via MAST. We imposed a quality check requiring photometry with `psfQfPerfect` > 0.95, yielding 73 points in *griz*, with surveying dates between 2010 February and 2015 February. We plot on a relative flux scale the PSF-extracted magnitudes normalized to their mean AB magnitude for each bandpass (J. L. Tonry et al. 2012) reported in Table 1.

CRTS. CRTS (A. J. Drake et al. 2009) is a multitelescope optical transient survey. We queried CRTS DR2 photometry through a cone search[10] on the J2000 coordinates of

[8] https://irsa.ipac.caltech.edu/data/ZTF/docs/ztf_zfps_userguide.pdf

[9] https://fallingstar-data.com/forcedphot/

[10] http://nunuku.caltech.edu/cgi-bin/getcssconedb_release_img.cgi

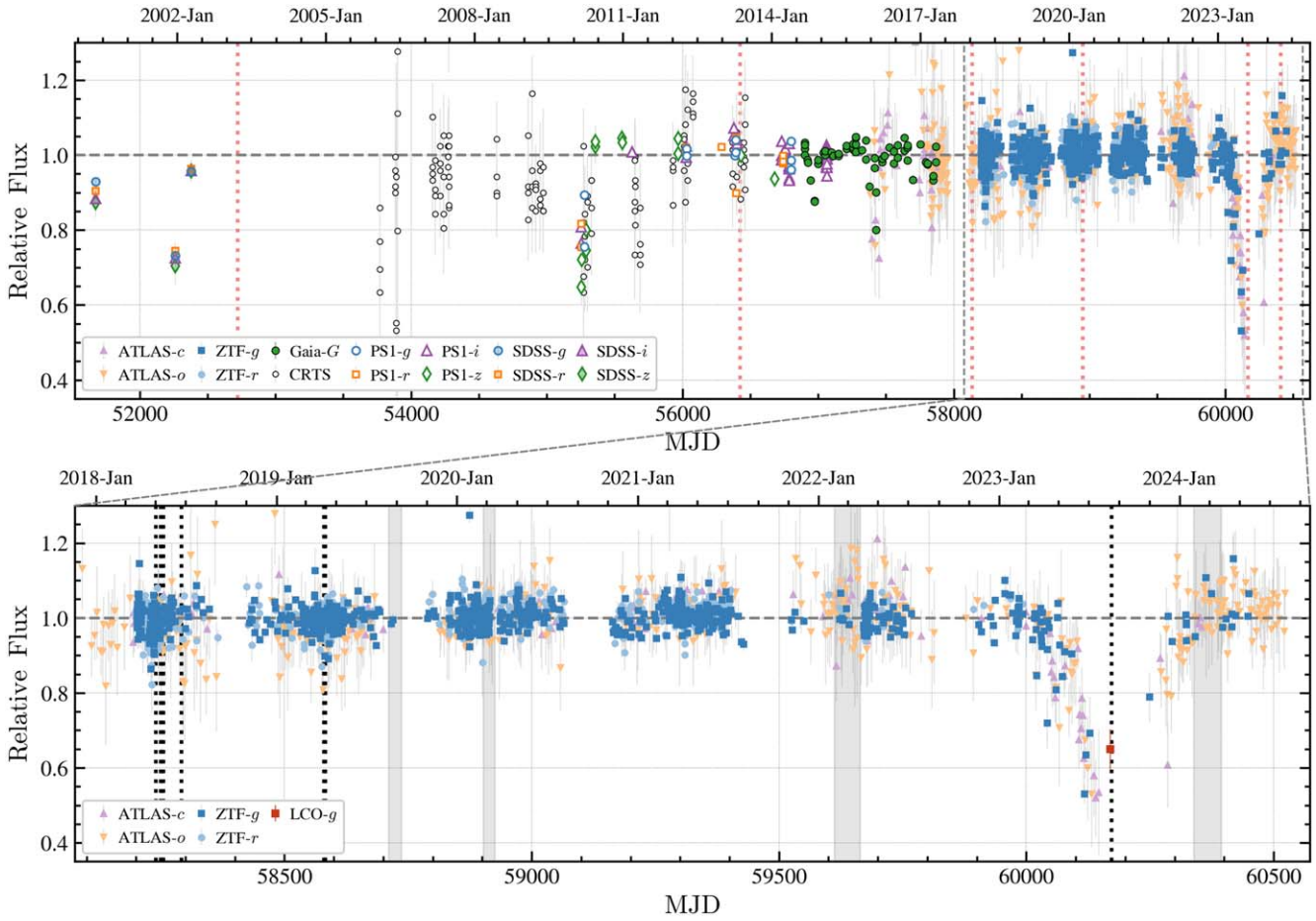

Figure 1. The top panel shows survey photometry for SBSS 1232+563, detailed in Section 2, spanning 2000–2024, which shows sporadic, deep dips. Low-resolution optical spectroscopy coincides with vertical dashed red lines, including a spectrum in 2023 collected in transit (see Section 4). The bottom panel shows a zoom in from 2018 to mid-2024. The deepest dip began in roughly 2023 April and extended until roughly 2024 January (more than 8 months), assuming the object remained in transit while it was not visible behind the Sun. The observing windows of high-speed photometric follow-up from McDonald Observatory (detailed in Section 3.1) are marked with vertical dashed black lines. Observational coverage during six sectors with TESS (further discussed in Section 3.2) is shown by gray shaded regions.

Table 1
Median Survey Filter Photometry

Survey	Date Range	Filter	λ_{cen} (nm)	Median (mag)
ZTF	2018−2024	*g*	481	18.03
		r	644	18.20
		i	752	18.44
ATLAS	2015−2024	*c*	518	18.05
		o	663	18.28
Gaia	2014−2017	*G*	673	18.04
PS1	2010−2015	*g*	487	17.95
		r	622	18.14
		i	755	18.35
		z	868	18.55
CRTS	2006−2013	*V*	550	18.01

Note. Catalina Real-Time Transient Survey (CRTS) photometry is unfiltered but the CCD response creates an effective λ_{cen} near the *V* band (A. J. Drake et al. 2013).

SBSS 1232+563, yielding 134 unblended epochs in the unfiltered (effective *V* band) from 2006 February through 2013 June. We only include the 20 epochs after MJD 56100 to calculate the median CRTS magnitude, as most of the previous epochs appear to be taken in transit.

SDSS. The earliest photometry analyzed here was collected by SDSS on 2000 May, with two other epochs on 2001 December and 2002 April. We acquired *ugriz* photometry at these epochs through an SQL query for `thingID` = 512173411. To put these SDSS photometry onto a consistent flux scale, we apply AB zero-point offsets ($u_{AB} = u_{SDSS} - 0.040$, $i_{AB} = i_{SDSS} + 0.015$, and $z_{AB} = z_{SDSS} + 0.030$, with no correction in *g* and *r*, as defined in D. J. Eisenstein et al. 2006) to the individual magnitude measurements before converting them to fluxes normalized to the respective PS1 mean magnitude (since it appears most SDSS photometry was taken in relatively deep transit).

Las Cumbres Observatory network (LCOGT). Seeing SBSS 1232+563 enter transit, we proposed for additional monitoring with LCOGT. We obtained 3×60 s exposures in the *g* band on 2023 August 13 from the 1.0 m telescope at Tenerife North in $2\farcs1$ seeing, which confirmed SBSS 1232 +563 to be $g = 18.51 \pm 0.06$ mag, more than 30% dimmer than the ZTF *g* median flux baseline.

WISE. We inspected near-infrared photometry of SBSS 1232 +563 from WISE at 3.4 μm (W1 band) and 4.6 μm (W2 band) from the NEOWISE mission (A. Mainzer et al. 2014). We queried the single-exposure image (hereafter referred to as L1b) photometry published within the 2024 NEOWISE data release

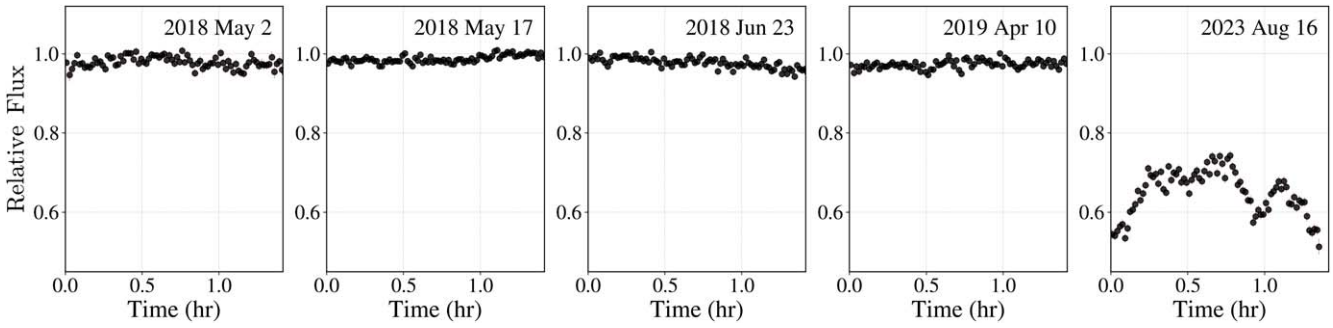

Figure 2. The first 1.4 hr for five separate nights of high-speed photometry of SBSS 1232+563 from the ProEM instrument on the 2.1 m Otto Struve Telescope at McDonald Observatory. The left four panels were all collected out of transit and are representative of our five other epochs from 2018 to 2019, while the right panel was collected in 2023 August in deep transit and shows considerably more short-term variability. All data have been binned to 1 minute and the closest measured nightly flux from Figure 1 has been subtracted.

from IRSA using `unTimely` (A. M. Meisner et al. 2023). unWISE coadds from the 2024 NEOWISE data release have yet been released, preventing us from reproducing the analysis from J. A. Guidry et al. (2024). We follow the methodology of J. A. Guidry et al. (2024) and convert the queried W1 and W2 Vega magnitudes from the NEOWISE era (2013–2023) to fluxes in units of μJy using the published conversions and subsequently sigma clip the photometry within a given epoch to 3σ for each bandpass, which we bin into single measurements. We estimate errors on our photometry by taking the ratio of the standard deviation of the clipped photometry to the square root of the number of measurements at that epoch. We do not include the L1b photometry in Figure 1 due to the large point-to-point (P2P) scatter (>20%).

3. High-speed Photometric Follow-up

Initially motivated by the inflated Gaia DR2 photometric uncertainties (J. Hermes et al. 2018), we densely observed SBSS 1232+563 over several nights in 2018 May and again in 2019 April, as detailed in Section 3.1, with epochs marked as dashed black lines in Figure 1. Additionally, the object is well-enough isolated that TESS produces useful photometry. Those observations are outlined in Section 3.2.

3.1. McDonald Observatory Time-series Photometry

We collected high-speed follow-up time-series photometry of SBSS 1232+563 for a total of more than 37.5 hr using the ProEM frame-transfer photometer mounted on the 2.1 m Otto Struve Telescope at McDonald Observatory. Our 10 individual epochs are summarized in Table 2. To reduce sky noise, we use a broad-bandpass, red-cutoff BG40 filter for all observations, which has a similar effective wavelength as the g filter. As indicated by the vertical lines in Figure 1, all of these epochs in 2018 and 2019 were taken outside of a deep transit event; only our 2023 August observations were collected in transit.

J. A. Guidry et al. (2021) showed roughly 4 hr from one of these McDonald runs from the night of 2019 April 9 in their Figure 6. We show five additional light curves in Figure 2. All data were collected in good conditions, with seeing generally $<1\farcs5$. We follow the reduction routine from J. A. Guidry et al. (2021) by executing standard IRAF routines to dark subtract and flat-field, running `CCD_HSP` (A. Kanaan et al. 2002) to do circular aperture photometry over a series of radii from 0.5 to 10.0 pixels, and using `phot2lc` (Z. Vanderbosch 2023) to extract the light curve that minimizes the average P2P scatter.

Table 2
Journal of 2.1 m McDonald High-speed Photometry

UT Date	Duration (hr)	Seeing ($''$)	Ap. (pixel)	Exp. (s)	P2P (%)	ΔFlux (%)
2018 May 2	1.76	1.4	3.5	20	2.3	6.2
2018 May 12	3.42	1.3	4.0	20	1.2	6.9
2018 May 14	4.37	1.6	4.5	20	1.7	6.2
2018 May 15	4.62	1.5	4.0	30	1.2	5.5
2018 May 17	4.01	1.0	3.5	10	1.1	3.2
2018 Jun 23	2.37	1.1	3.0	20	1.3	5.0
2019 Apr 7	2.50	1.7	5.0	30	1.3	5.3
2019 Apr 9	7.13	1.3	3.5	30	1.0	3.3
2019 Apr 10	6.01	1.4	3.5	30	1.2	5.4
2023 Aug 16	1.36	1.2	3.5	5	2.6	20.8

Note. Ap. is the radius in pixels of the circular aperture drawn for our photometry extraction. P2P is the average P2P scatter of each light curve binned to 1 minute cadence. ΔFlux is the total flux excursion within the first 1 hr of the 1 minute binned light curve.

We performed differential photometry on a stable, nearby comparison star. Some of our longer runs suffer from some differential extinction (there is an airmass-dependent color difference in our blue target and the available comparison stars). We usually divide out a second-order polynomial to account for these airmass changes over longer (>4 hr) runs (S. E. Thompson & F. Mullally 2009). Since we are interested in directly comparing possible short-period, transit-induced variability in our light curves, we do not divide out any low-order polynomial terms.

Figure 2 shows five representative light curves, each to the same scale, showing the dramatic short-period, in-transit variability observed in 2023 August. We coadd all light curves into 1 minute bins to help directly compare each run. Despite suggestions of variability, we did not see evidence for major transits deeper than roughly 7% in the 2018 and 2019 light curves of SBSS 1232+563.

Light-curve metrics detailed in Table 2 measure the P2P scatter of these 1 minute bins. We also measure the P2P variability for the first 1 hr of each run (ΔFlux), measuring the maximum flux excursion from the highest and lowest point of these 1 minute binned light curves. The McDonald/ProEM measurements reveal that the light curve collected in deep transit in 2023 August shows at least three times more extreme short-term (minutes-long) variability than any other epoch of

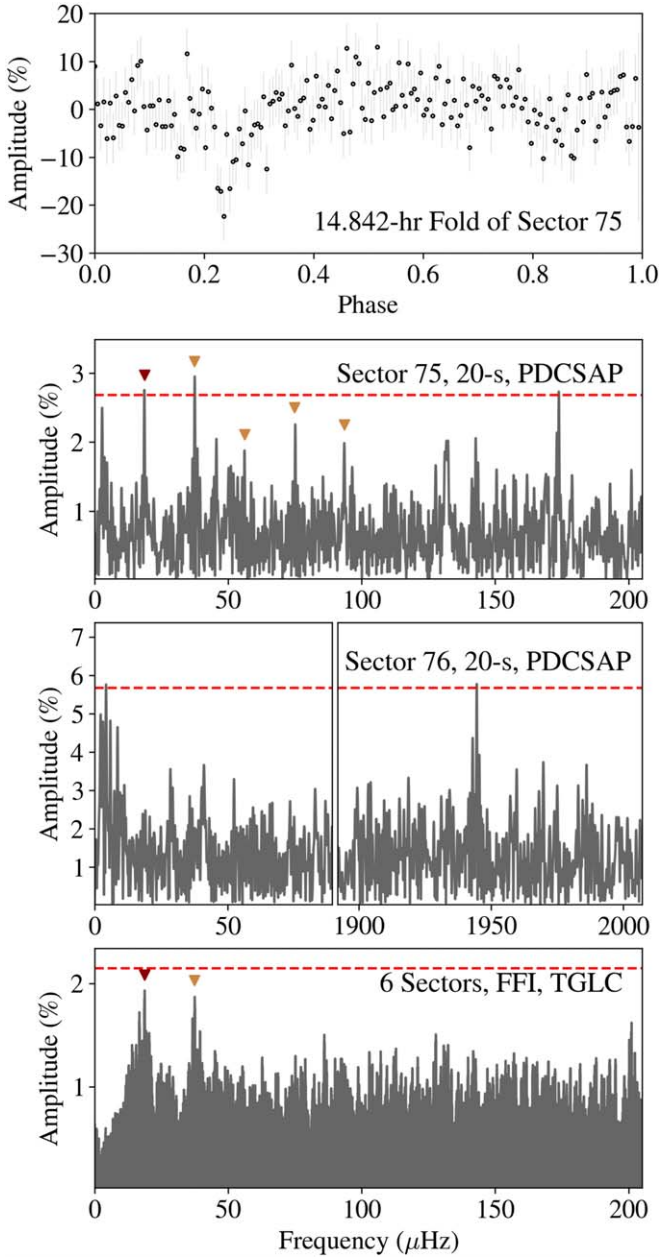

Figure 3. The top panel shows 180 phase bins of the light curve of SBSS 1232+563 from TESS Sector 75 folded at 14.842 hr. The panels below show Lomb–Scargle periodograms of various TESS data. The second panel shows a periodogram of 20 s data from Sector 75, the highest-quality TESS data, where we detect significant signals at 14.842 hr (18.7 μHz), the second harmonic at 7.421 hr, and a (likely) nonharmonic signal at 95.8416 minutes. We mark the fundamental with a maroon triangle and integer harmonics as orange triangles. The dashed red line is a bootstrapped 0.1% false-alarm probability (above which peaks are formally significant). The third panel shows 20 s data from Sector 76. No significant peaks related to the 14.842 hr fundamental are seen, though there is a significant signal at 1944.5 μHz (8.57 minutes) of uncertain origin. The bottom panel shows all FFI data. No formally significant signals are detected in earlier FFI data, but the 14.842 hr fundamental and its second harmonic are marginally detected in data from all six sectors.

observation in 2018 and 2019, all of which were collected out of major transit (see black dashed lines in Figure 1).

3.2. Coherent Signals Present in TESS

Photometry from SBSS 1232+563 was captured over six sectors by TESS (G. R. Ricker et al. 2015). Full-frame image (FFI) data were collected every 30 minutes during the first two sectors (Sectors 15 and 22), observed during most of 2019 August and then most of 2020 May. The cadence of the FFI images decreased to 10 minutes during observations in Sectors 48 and 49, covering almost all of 2022 February to 2022 March. The FFI exposure times decreased again, to 200 s, for data collected in Sectors 75 and 76 (observed from 2024 February to 2024 March).

Table 3
Significant Signals in TESS Photometry

ID	Period (hr)	Frequency (μHz)	Amplitude (%)
TESS 20 s Cadence, Sector 75			
f_1	14.842 ± 0.035	18.715 ± 0.044	2.56 ± 0.49
$2f_1$	7.4211 ± 0.0084	37.431 ± 0.042	2.67 ± 0.49
f_2	1.59736 ± 0.00014	173.898 ± 0.015	2.84 ± 0.19
TESS 20 s Cadence, Sector 76			
f_3	0.1428515 ± 0.0000030	1944.521 ± 0.041	5.8 ± 1.0

In addition to FFI data, TESS targeted SBSS 1232+563 (cataloged as TIC 950506740, $T = 18.1$ mag) with 20 s cadence data. The white dwarf is incredibly faint for the effective 10 cm aperture of TESS, but it is in a relatively uncrowded field, which still makes the TESS photometry useful; the target contributes more than 35% of the flux in the 5 pixel extraction aperture in Sector 75 as well as the 6 pixel aperture for Sector 76. There is only one ($G = 20.6$) object in Gaia within 30″ of SBSS 1232+563, 21.″5 to the SE. The nearest brighter stars are a $G = 16.7$ mag star 55.″7 to the N and a $G = 17.9$ mag star 58.″0 to the W.

We extracted all six sectors of FFI data using PSF fitting of background Gaia sources using the `TESS-Gaia Light Curve` software (T. Han & T. D. Brandt 2023). For our last two sectors we also analyzed the 20 s light curves from the Presearch Data Conditioning Simple Aperture Photometry (PDCSAP) fluxes produced by the Science Processing Operations Center and hosted on MAST (J. M. Jenkins et al. 2016). Sectors 75 and 76 suffer from significant scattered light, mostly from the Earth, yielding a poor duty cycle of 44.9% and 38.8%, respectively.

We show in the middle panels of Figure 3 Lomb–Scargle periodograms of the 20 s PDCSAP light curves. We also show the empirical 0.1% false-alarm probability for each sector, above which peaks have a <0.1% chance to arise from noise, which were bootstrapped from 10,000 periodograms of shuffling the fluxes but keeping the time sampling the same (e.g., K. J. Bell et al. 2019).

Sector 75 reveals multiple significant signals: a first and second harmonic at $f_1 = 18.715$ μHz (14.842 hr) and $2f_1 = 37.431$ μHz (see Table 3). Peaks are also present at the third, fourth, and fifth harmonics of the 14.842 hr fundamental signal, but they fall below the 0.1% false-alarm threshold. These harmonics arise to reproduce the nonsinusoidal structure shown in the folded light curve in the top panel of Figure 3. Sector 75 also reveals a significant signal at $f_2 = 173.898$ μHz (95.8416 ± 0.0085 minutes), which does not appear harmonically related to the 14.842 hr fundamental. All significant peaks exceed 2.68% amplitude (the false-alarm line). Sector 75 has the smaller P2P scatter and flux uncertainties than the other 20 s cadence data in Sector 76, and was collected from 2024

January 30 to 2024 February 26, close to when the star returned to near-quiescent flux levels after the deep 2023 transit.

Data immediately thereafter in Sector 76 do not reveal significant peaks at any harmonics of the 14.842 hr fundamental signal. There is a formally significant peak at low frequency (4.35 μHz) that, at 2.66 days, is likely connected to background variability. More notable, there is a significant peak at $f_3 = 1944.521$ μHz (8.57 $\pm$ 0.14 minutes, see Table 3). If harmonically related to the 14.842 hr fundamental, this would be the 103rd or 104th harmonic of f_1; although high harmonics of debris orbital frequencies have been observed in transiting debris systems (J. Farihi et al. 2022), we merely suggest such a connection at this time.

We use `TESS_localize` (M. E. Higgins & K. J. Bell 2023) to vet the origin of the significant signals in the 20 s TESS data. In Sector 75, we find that the first five harmonics of $f_1 = 18.715$ μHz have a relative likelihood of 1.000 (p-value = 0.044[11]) of arising from SBSS 1232+563. In another independent test, we find the signal $f_2 = 173.898$ μHz has a relative likelihood of 1.000 (p-value = 0.055) of arising from SBSS 1232+563. In Sector 76, we find the $f_3 = 1944.521$ μHz signal is confidently associated with SBSS 1232+563, with a relative likelihood of 1.000 (p-value = 0.962). We have also performed periodograms on the background flux values of our PDCSAP light curves and do not find peaks at $f_1 - f_3$ or their harmonics.

If persistent, such high-amplitude signals should show up in our other data sets. However, we do not identify periodic signals in either the ZTF g, r, and combined $g + r$ photometry, nor in the ATLAS c, o, and combined $c + o$ photometry. Only aliases from the diurnal survey pattern appear. We similarly do not identify signals at 14.842 hr, 95.8416 minutes, or 8.57 minutes in the periodograms of either of the combined 2018 May and 2019 April McDonald ProEM light curves. We do, however, find that the combined McDonald 2018 May light curve has a best period of 8.616 hr, found from a period search using the Stellingwerf phase-dispersion minimization (R. F. Stellingwerf 1978) period-finding algorithm as implemented in `astrobase` (W. Bhatti et al. 2018). This trial period is a marginally better fit than the second- and third-best periods of 6.456 hr and 7.512 hr, respectively. It is possible that the 7.512 hr signal is an alias of the half harmonic of the 14.842 hr signal seen in TESS, but none of these periods are formally significant.

That we cannot see the high-amplitude signals at 14.842 hr, 95.8416 minutes, and 8.57 minutes observed by TESS in other data sets challenges that these are intrinsic astrophysical variability toward SBSS 1232+563. However, the Sector 75 and 76 TESS data are some of the only photometry collected very near if not in the transit event that began in 2023 April. It is possible these signals are transient and only manifest in transit. Our 1.4 hr of photometry in 2023 August from McDonald Observatory taken in deep transit are too short to confirm any periodic signals.

4. Search for Spectroscopic Changes

There is considerable spectroscopy of SBSS 1232+563, some archival and spanning more than two decades and taken both in and out of transit, marked as six separate dashed gray lines in Figure 1. Each of these spectra, focused around the calcium H and K lines, are shown in Figure 4. Basic properties of the spectra are outlined in Table 4.

SDSS. The oldest spectrum of SBSS 1232+563 was collected on 2003 March 23 and released as part of SDSS DR4 (D. J. Eisenstein et al. 2006), collected with the original SDSS spectrograph. SDSS revisited the white dwarf two more times, on 2013 May 14 and 2018 January 17; the latter two spectra were collected with the BOSS spectrograph (A. S. Bolton et al. 2012). All SDSS spectral data were obtained via SciServer (M. Taghizadeh-Popp et al. 2020).

Hobby–Eberly Telescope Dark Energy Experiment (HETDEX). SBSS 1232+563 was observed on 2020 April 12[12] by HETDEX (G. J. Hill et al. 2008). The white dwarf was included in the second data release of the HETDEX Survey, which performed a reextraction of HETDEX stellar spectra to account for Gaia proper motions (K. Hawkins et al. 2021).

Double Spectrograph (DBSP). When SBSS 1232+563 entered transit in 2023 we triggered spectroscopy with DBSP on the 200 inch telescope at Palomar Observatory (J. B. Oke & J. E. Gunn 1982). Our two 15 minute exposures were collected using a 1.″5 slit on 2023 August 13 using the 316-line grating blazed at 7500 Å for the red arm and the 600-line grism blazed at 4000 Å on the blue arm; due to a CCD defect on the red arm, there is a gap in coverage from 5550 to 5730 Å. We reduced and coadded the spectra using `DBSP-DRP`,[13] which is built upon the `PypeIt` package (J. Prochaska et al. 2020). This was our only available spectroscopic observation of SBSS 1232+563 in deep transit.

Low-Resolution Imaging Spectrometer (LRIS). Our final spectrum in this work was collected using LRIS mounted on the Keck I 10 m telescope on Maunakea (J. B. Oke et al. 1995; C. Rockosi et al. 2010). We collected two 10 minute exposures on 2024 April 10 using a 1.″0 slit with the D560 dichroic. We used the 600-line mm^{-1} grism blazed at 4000 Å on the blue arm and the 400 line mm^{-1} grating blazed at 8500 Å on the red arm. We reduced and coadded the spectra using the LRIS automated reduction pipeline (D. A. Perley 2019) using the flux standard G191-B2B.

We analyze the abundances (and possible abundance changes) of the low-resolution spectra of SBSS 1232+563 using `cecilia`, a machine learning–based pipeline for measuring the elemental abundances of He-rich white dwarfs (M. Badenas-Agusti et al. 2024). In fact, the most recent SDSS spectrum of SBSS 1232+563 collected in 2018 January was used as a test case in Section 5.2 of M. Badenas-Agusti et al. (2024). We extend that analysis to all low-resolution spectra in Figure 4.

Table 4 summarizes our MCMC best-fit parameters using `cecilia`. We follow identically the steps outlined in Section 5.2 of M. Badenas-Agusti et al. (2024), fixing the atmospheric parameters ($T_{\rm eff} = 11{,}787$ K, $\log g = 8.30$) based on those of S. Coutu et al. (2019), although we caution that these parameters, especially the $\log g$, likely have extra uncertainty due to the variable photometry of the system and the most accurate mass and temperature will require a more detailed analysis. In summary, before each fit, we slightly processed all spectra by removing regions around known skylines and

[11] The p-values from `TESS_localize` estimate the fraction of fit locations that would have been less likely than the actual fit location under the hypothesis that each source in the field is the variable source, such that higher p-values are more reliable (M. E. Higgins & K. J. Bell 2023).

[12] Almost no observatories besides HET were operating in 2020 April due to the COVID-19 pandemic.

[13] https://dbsp-drp.readthedocs.io/en/stable/index.html

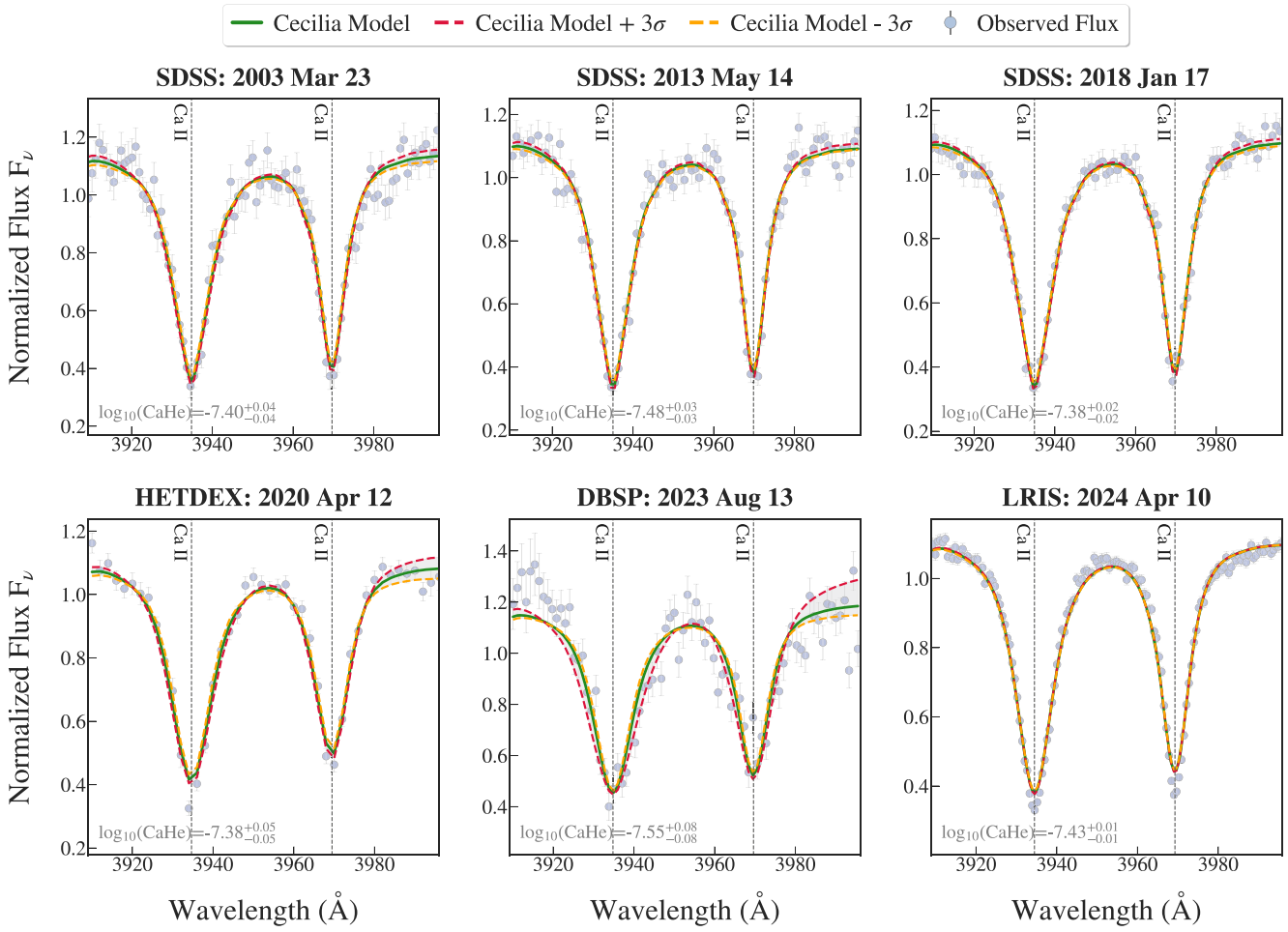

Figure 4. Six epochs of low-resolution spectroscopy collected on SBSS 1232+563, at epochs denoted in Figure 1. We zoom in here on the calcium H and K lines, with the best-fit `cecilia` (M. Badenas-Agusti et al. 2024) model overplotted in green. The values reported for each epoch include the statistical Markov Chain Monte Carlo (MCMC) uncertainties; full abundances including systematic uncertainties for all detected metals are detailed in Table 4.

tellurics. We then executed individual MCMC runs with 50 walkers, 3000 links, and a 20% burn-in, imposing wide chondritic priors on elements that are typically easy to detect (Ca, Mg, Fe, O, and Si; prior width of 2 dex), and narrower priors on the remaining elements (Ti, Cr, Mn, and Ni: 0.5 dex). This configuration was sufficient to achieve convergence and took between 1.8 hr (HETDEX) and 6.2 hr (LRIS) to complete.

The uncertainties given in Table 4 reflect adding the statistical MCMC uncertainties ($\sigma_{\rm stat,MCMC}$), systematic uncertainties from `cecilia`'s machine learning–based interpolation ($\sigma_{\rm sys,ML}$, as detailed in Table 5 of M. Badenas-Agusti et al. 2024), and systematic atmospheric model uncertainties ($\sigma_{\rm sys,model} = 0.10$ dex) in quadrature. We assume that an element is detected when its total uncertainty is less than 0.20 dex and confirm this detectability threshold through a visual inspection of the spectra. In Table 4, we report 3σ upper limits on any elements with total uncertainties above 0.20 dex. Our best 3σ upper limits for Cr, Mn, and Ni come from our LRIS spectrum: $\log_{10}({\rm Cr/He}) < -7.98$, $\log_{10}({\rm Mn/He}) < -8.15$, and $\log_{10}({\rm Ni/He}) < -6.92$, respectively.

When detected, the measured elemental abundances all agree within 1σ at all epochs, and are always within 1σ consistent with the abundances determined from the highest-resolution spectra of SBSS 1232+563 collected by Keck/HIRES presented in S. Xu et al. (2019), which we also include in Table 4. The abundance measurements found by `cecilia` for Ca at all six epochs agree within 1σ with the value of $\log_{10}({\rm Ca/He}) = -7.41 \pm 0.06$ from the S. Coutu et al. (2019) analysis of the 2013 SDSS spectrum.[14]

The six low-resolution spectra analyzed here show remarkable consistency in the observed elemental abundances (especially Ca, Mg, Fe, O, and Si). All elements except H have long (>0.3 Myr) settling times (C. Paquette et al. 1986). It is worth noting that the highest-resolution ($R = 40{,}000$) spectra from S. Xu et al. (2019) show no extra broadening or other evidence of circumstellar absorption lines.

5. Discussion and Conclusions

We have detected sporadic, extended transits in multicolor optical photometry of the metal-rich white dwarf SBSS 1232+563, most likely caused by occultations due to disrupted rocky debris. Dense observations from the transient surveys ZTF and ATLAS show that for more than 5 yr (from 2018 January to 2023 January) the white dwarf was within a few

[14] We note that all but one Ca measurement is $>1\sigma$ more abundant than Keck/HIRES spectra from 2015 April 11 and 2016 April 1, found by S. Xu et al. (2019) to have $\log_{10}({\rm Ca/He}) = -7.69 \pm 0.05$ determined from an independent analysis not using `cecilia`. This discrepancy does not show up for any other elements.

Table 4
Spectroscopic Information and Abundance Measurements of SBSS 1232+563 at Different Epochs

Value	APO (SDSS)	APO (BOSS)	APO (BOSS)	McD (HETDEX)	Palomar (DBSP)	Keck (LRIS)	S. Xu et al. (2019)
Observation Date	2003 Mar 23	2013 May 14	2018 Jan 17	2020 Apr 12	2023 Aug 13	2024 Apr 10	2015−2017
Wavelengths (Å)	3800–9200	3610–10140	3610−10140	3500−5500	3200−10800	3150−10270	3200−10000
Effective Resolution	1800	2000	2000	750	1000	1100	40,000
S/N	34.4	48.6	51.8	34.9	17.9	158.4	68.0
Fraction of Flux	∼95% (within 1 yr)	99% (within 1 day)	99% (within 1 day)	100% (within 1 day)	65% (within 1 day)	97% (within 1 day)	94%−100%
$\log_{10}$(Ca/He)	−7.40 ± 0.13	−7.48 ± 0.13	−7.38 ± 0.12	−7.38 ± 0.13	−7.55 ± 0.15	−7.43 ± 0.12	−7.69 ± 0.05
$\log_{10}$(Mg/He)	−6.01 ± 0.12	−6.07 ± 0.12	−6.03 ± 0.11	−6.06 ± 0.12	<−6.09	−6.02 ± 0.11	−6.09 ± 0.05
$\log_{10}$(Fe/He)	−6.37 ± 0.15	−6.27 ± 0.13	−6.54 ± 0.14	$-6.37^{+0.16}_{-0.15}$	<−5.73	−6.21 ± 0.12	−6.45 ± 0.11
$\log_{10}$(O/He)	<−4.80	$-5.13^{+0.18}_{-0.17}$	$-5.02^{+0.18}_{-0.17}$	<−3.99	<−4.40	−5.32 ± 0.14	−5.14 ± 0.15
$\log_{10}$(Si/He)	$-6.28^{+0.16}_{-0.17}$	−6.23 ± 0.14	$-6.40^{+0.15}_{-0.16}$	<−6.01	<−5.63	−6.32 ± 0.13	−6.36 ± 0.13
$\log_{10}$(Ti/He)	<−8.02	<−8.61	<−8.47	<−8.23	<−7.72	−8.86 ± 0.13	−8.96 ± 0.11
$\log_{10}$(H/He)	<−5.41	−5.61 ± 0.13	$-5.82^{+0.16}_{-0.18}$	<−4.97	<−5.30	−5.63 ± 0.11	−5.90 ± 0.15

Note. All analyses made with `cecilia` (M. Badenas-Agusti et al. 2024) except for those from Keck HIRES/ESI data by S. Xu et al. (2019), who perform a line-by-line χ^2 approach that applies the same weights to each spectral feature as described in P. Dufour et al. (2012). The S/N is measured per resolution element in the range from 5200 to 5300 Å. Fraction of flux shows the measured relative flux from Figure 1 and when that measurement was made compared to the spectroscopy.

percent of constant flux. SBSS 1232+563 then entered a roughly 8 month long, nearly 50% deep transit for most of 2023. The long duration of the event suggests an extended cloud is likely required, which follows a highly eccentric orbit with an extreme apastron.

High-speed photometry from McDonald Observatory shows that there is higher-amplitude, short-term (minutes to hours) variability in transit (in 2023) compared to data taken out of transit (in 2018 and 2019; Figure 2). ZTF J0923+4236, a white dwarf that shows sporadic transits from planetary debris at weeks-long intervals, similarly shows heightened short-timescale variability in transit, relative to its near-flat out-of-transit flux baseline (A. Aungwerojwit & V. S. Dhillon 2024). This suggests that the transit events are an inhomogeneous cloud of debris unevenly blocking the white dwarf.

TESS data collected out of transit (2019, 2020, and 2022) do not show significant variability, but the TESS data from 2024 collected just after the large dimming in event from 2023 reveal several significant periodicities. We have yet to confidently identify the physical origin of the periodic signals, but they appear intrinsic to SBSS 1232+563.

It is possible a surface inhomogeneity (spot) is responsible for the longest TESS photometric period at 14.842 hr; the shorter signals at 95.8416 minutes and 8.57 minutes would be extremely fast for a white dwarf rotation period (J. J. Hermes et al. 2017a). However, spotted white dwarfs tend to be fairly sinusoidal, rarely revealing higher than the third harmonic of the rotation period (e.g., J. J. Hermes et al. 2017b; D. J. Wilson et al. 2020). Sector 75 shows at least five harmonics of the 14.842 hr fundamental signal. The morphology of the periodogram is far more reminiscent of the many harmonics seen trying to reproduce the nonsinusoidal shape of transiting debris (Z. P. Vanderbosch et al. 2021; J. Farihi et al. 2022).

Should the 14.842 hr signal we detect in TESS Sector 75 be the orbital period of the debris transiting SBSS 1232+563, it would be the fifth measured orbital period of transiting debris at a white dwarf: WD 1145+017—4.49 hr (A. Vanderburg et al. 2015), ZTF J0328−1218—9.937 hr and 11.2 hr (Z. P. Vanderbosch et al. 2021), WD 1054−226—25.02 hr (J. Farihi et al. 2022), and ZTF J0139+5245—≈107 days (Z. Vanderbosch et al. 2020). Altogether, this spectrum of periods may be evidence for the gradual evolution of tidally disrupted material from highly eccentric, extended, long-period ($\gtrsim 10^2$ days) orbits to closer-in, more circular orbits with periods comparable to the circular orbit at the tidal disruption radius for a typical white dwarf (e.g., M. G. Brouwers et al. 2022), $P_{\rm orbit,TD} \sim 4.5$ hr.

In addition to the dramatic 2023 dimming event, Figure 5 shows that SBSS 1232+563 reveals further extended (>3 month) transits from PS1 data, deepest around 2010 April, as well as a transit in Gaia DR3, deepest around 2016 January. There does not appear to be a coherent recurrence timescale to these extended events, which recur roughly every ∼6–8 yr. Fixed patterns in the circumstellar gas in some white dwarf debris disks are measured to precess on years-long timescales (C. J. Manser et al. 2016; P. W. Cauley et al. 2018), despite also showing shorter-period signals (e.g., C. J. Manser et al. 2019). However, the lack of coherence to the deep transits complicates precession as the core driver of the long-period recurrence of transits toward SBSS 1232+563.

We attempted to constrain the grayness of the debris transiting SBSS 1232+563. We emulate the analysis of L. A. Hillenbrand et al. (2022) to search for trends in the $g-r$ colors among observations taken within 1 day intervals in ZTF. We fit two lines to the g versus $g-r$ values: one with zero slope that would support a colorless, gray transit, and one where we allow the slope to vary. We find the reduced χ^2 between the flat and sloped lines to be statistically consistent, with slight preference to the sloped line ($\chi^2_{\rm sloped} = 2.5$ versus $\chi^2_{\rm flat} = 3.2$). We further search for a trend between the ZTF g and ATLAS o photometry also within 1 day intervals, aiming to better resolve the 2023 transit with greater color contrast than can be achieved with $c-o$. Again, the reduced χ^2 of the sloped line is preferred to the flat line, but are still comparable in value ($\chi^2_{\rm sloped} = 8.3$ versus $\chi^2_{\rm flat} = 11.3$). It does not appear there is a significant color term to the transits.

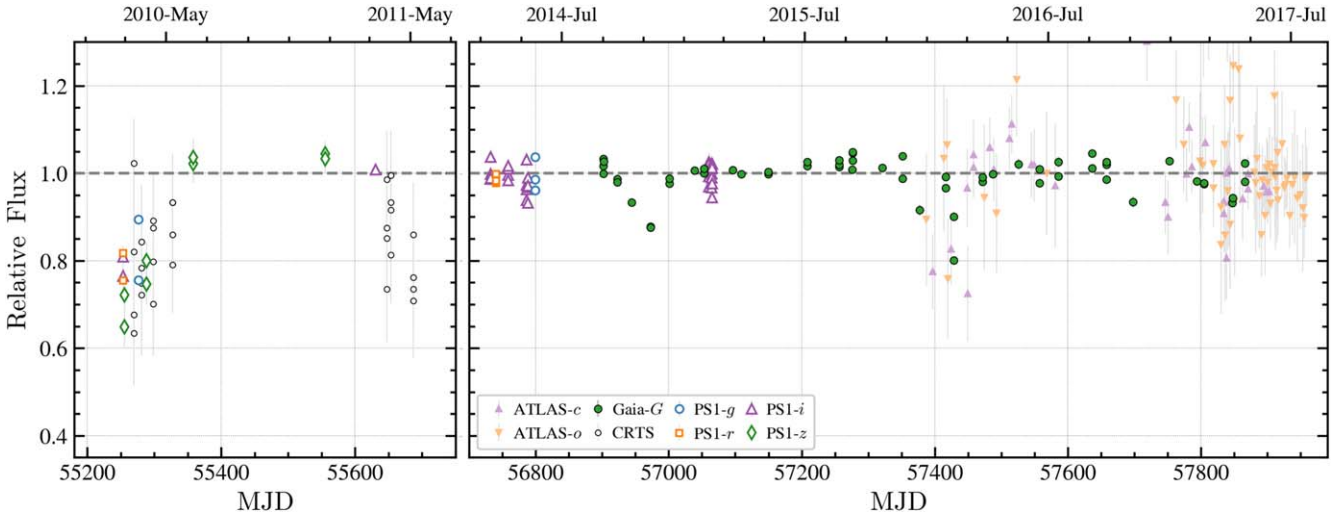

Figure 5. Survey photometry for SBSS 1232+563 centered around additional transits around MJD 55300 (2010 April) detected by PS1 in the left panel and MJD 57410 (2016 January) detected by Gaia in the right panel. All points have uncertainties; some error bars are smaller than the points themselves.

More stringently, the SDSS $u-r$, $u-i$, $g-r$, and $g-i$ colors are all consistent to within their associated uncertainties across the three SDSS photometric epochs. All bands were observed within 5 min at each epoch. Figure 1 shows all three epochs at different transit depths, one 5% deep and one nearly 30% deep. The standard deviation of the color term for the three epochs is smallest for $g-r$ and is 0.024 mag, in line with the average $g-r$ photometric uncertainty of 0.027 mag. The SDSS test suggests that the material is mostly gray, in line with other white dwarfs harboring transiting debris (R. Alonso et al. 2016; P. Izquierdo et al. 2018).

We do not detect significant variability of the IR excess from the warm, dusty debris disk around SBSS 1232+563, although its faintness would require very large (>20%) changes to manifest as variable from the NEOWISE monitoring (J. A. Guidry et al. 2024). NEOWISE observed SBSS 1232 +563 on 2023 May 4, which showed a 36% and 26% decrease in flux in W1 and W2, respectively, relative to the mean flux weighted to the photometric uncertainties. However, the large uncertainties means that these points only deviate by 2.5σ in W1 and 1.9σ in W2 from their respective averages. An IR dimming in transit would be consistent with gray transits. It could also suggest the extended events are unlikely collisionally driven, as they would generate a commensurate IR brightening (e.g., A. Swan et al. 2021).

Spectroscopy collected at various times and transit depths do not show significant abundance changes in the rock-forming elements (Ca, Mg, Fe, and Si) nor volatile elements (O and H) during various transit depths, although our in-transit measurements have the worst S/N and fewest species confidently detected. Triggering higher-resolution spectroscopy during a future deep transit could put much more stringent limits on the lack of in-transit spectroscopic variability in SBSS 1232+563, motivating monitoring of the system to see if there is optically thick circumstellar gas between us and the white dwarf (akin to the changing absorption features observed by Z. Vanderbosch et al. 2020 toward the long-period transiting white dwarf ZTF J0139+5245).

The 25 yr light curve of SBSS 1232+563 in Figure 1 reveals that this transiting white dwarf can go for many years (perhaps half a decade) at quiescent flux levels before entering deep transit. As also noted by A. Aungwerojwit & V. S. Dhillon (2024), this long-term variability complicates accurate calculations of transit occurrence rates (L. van Sluijs & V. Van Eylen 2018; D. M. Rowan et al. 2019; A. Robert et al. 2024). This motivates extending the baseline for surveys like ZTF and ATLAS to keep watch for more transit events, and we eagerly await new facilities such as Rubin (Ž. Ivezić et al. 2019) and Roman (R. Akeson et al. 2019) to open this search for extended transits to orders of magnitude more faint white dwarf stars.

Acknowledgments

We thank the anonymous referee for constructive feedback that helped this work, Tim Cunningham for helpful discussions in the preparation of this manuscript, and J. W. Kuehne for observation support. This material is based upon work supported by the National Aeronautics and Space Administration under grant No. 80NSSC23K1068 issued through the Science Mission Directorate. Support for this work was in part provided by NASA TESS Cycle 6 grant 80NSSC24K0878. J.A.G. is supported by the National Science Foundation Graduate Research Fellowship Program under grant No. 2234657.

The ZTF forced-photometry service was funded under the Heising–Simons Foundation grant #12540303 (PI: Graham). This work has made use of data from the European Space Agency (ESA) mission Gaia (https://www.cosmos.esa.int/gaia), processed by the Gaia Data Processing and Analysis Consortium (DPAC; https://www.cosmos.esa.int/web/gaia/dpac/consortium). Funding for the DPAC has been provided by national institutions, in particular the institutions participating in the Gaia Multilateral Agreement. This paper includes data collected by the TESS mission. Funding for the TESS mission is provided by the NASA's Science Mission Directorate. The CSS survey is funded by the National Aeronautics and Space Administration under grant No. NNG05GF22G issued through the Science Mission Directorate Near-Earth Objects Observations Program. The CRTS survey is supported by the U.S. National Science Foundation under grant AST-0909182. Some of the data presented herein were obtained at Keck Observatory, which is a private 501(c)3 nonprofit organization operated as a scientific partnership among the California Institute of Technology, the University of California, and the National Aeronautics and Space Administration. The

Observatory was made possible by the generous financial support of the W. M. Keck Foundation. The authors wish to recognize and acknowledge the very significant cultural role and reverence that the summit of Maunakea has always had within the Native Hawaiian community. We are most fortunate to have the opportunity to conduct observations from this mountain.

S.X. is supported by NOIRLab, which is managed by the Association of Universities for Research in Astronomy (AURA) under a cooperative agreement with the National Science Foundation. M.L.K. and K.H. acknowledge support from the Wootton Center for Astrophysical Plasma Properties, a U.S. Department of Energy NNSA Stewardship Science Academic Alliance Center of Excellence supported under award numbers DE-NA0003843 and DE-NA0004149, and from the United States Department of Energy under grant DE-SC0010623. K.H. acknowledges support from the National Science Foundation grant AST-2108736. This research was improved by discussions at the KITP Program "White Dwarfs as Probes of the Evolution of Planets, Stars, the Milky Way and the Expanding Universe" supported by National Science Foundation under grant No. NSF PHY-1748958.

Facilities: PO:1.2m, ATLAS, Gaia, PS1, SO:1m, Sloan, LCOGT, WISE, NEOWISE, Struve, TESS, HET, Hale, Keck:I.

*S*oftware: astrobase (W. Bhatti et al. 2018), astropy (Astropy Collaboration et al. 2013, 2018), astroquery (A. Ginsburg et al. 2019), cecilia (M. Badenas-Agusti et al. 2024), lmfit (M. Newville et al. 2014), Matplotlib (J. D. Hunter 2007), NumPy (C. R. Harris et al. 2020), pandas (pandas development team 2020), SciPy (P. Virtanen et al. 2020), Period04 (P. Lenz & M. Breger 2005), phot2lc (Z. Vanderbosch 2023), and TESS_localize (M. E. Higgins & K. J. Bell 2023).

ORCID iDs

J. J. Hermes https://orcid.org/0000-0001-5941-2286
Joseph A. Guidry https://orcid.org/0000-0001-9632-7347
Zachary P. Vanderbosch https://orcid.org/0000-0002-0853-3464
Mariona Badenas-Agusti https://orcid.org/0000-0003-4903-567X
Siyi Xu (许偲艺) https://orcid.org/0000-0002-8808-4282
Malia L. Kao https://orcid.org/0000-0001-5745-3535
Antonio C. Rodriguez https://orcid.org/0000-0003-4189-9668
Keith Hawkins https://orcid.org/0000-0002-1423-2174

References

Akeson, R., Armus, L., Bachelet, E., et al. 2019, arXiv:1902.05569
Alonso, R., Rappaport, S., Deeg, H. J., & Palle, E. 2016, A&A, 589, L6
Astropy Collaboration, Price-Whelan, A. M., Sipőcz, B. M., et al. 2018, AJ, 156, 123
Astropy Collaboration, Robitaille, T. P., Tollerud, E. J., et al. 2013, A&A, 558, A33
Aungwerojwit, A., Gänsicke, B. T., Dhillon, V. S., et al. 2024, MNRAS, 530, 117
Badenas-Agusti, M., Viaña, J., Vanderburg, A., et al. 2024, MNRAS, 529, 1688
Bell, K. J., Córsico, A. H., Bischoff-Kim, A., et al. 2019, A&A, 632, A42
Bhatti, W., Bouma, L. G., & Wallace, J. 2018, Astrobase, v0.3.8, Zenodo, doi:10.5281/zenodo.1185231
Bicay, M. D., Stepanian, J. A., Chavushyan, V. H., et al. 2000, A&AS, 147, 169
Bolton, A. S., Schlegel, D. J., Aubourg, É., et al. 2012, AJ, 144, 144
Brouwers, M. G., Bonsor, A., & Malamud, U. 2022, MNRAS, 509, 2404
Brouwers, M. G., Buchan, A. M., Bonsor, A., et al. 2023, MNRAS, 519, 2663
Cauley, P. W., Farihi, J., Redfield, S., et al. 2018, ApJL, 852, L22
Chambers, K. C., Magnier, E. A., Metcalfe, N., et al. 2016, arXiv:1612.05560
Coutu, S., Dufour, P., Bergeron, P., et al. 2019, ApJ, 885, 74
Debes, J. H., Hoard, D. W., Wachter, S., Leisawitz, D. T., & Cohen, M. 2011, ApJS, 197, 38
Drake, A. J., Catelan, M., Djorgovski, S. G., et al. 2013, ApJ, 763, 32
Drake, A. J., Djorgovski, S. G., Mahabal, A., et al. 2009, ApJ, 696, 870
Dufour, P., Kilic, M., Fontaine, G., et al. 2012, ApJ, 749, 6
Eisenstein, D. J., Liebert, J., Harris, H. C., et al. 2006, ApJS, 167, 40
Eyer, L., Audard, M., Holl, B., et al. 2023, A&A, 674, A13
Farihi, J. 2016, NewAR, 71, 9
Farihi, J., Gänsicke, B. T., & Koester, D. 2013, Sci, 342, 218
Farihi, J., Hermes, J. J., Marsh, T. R., et al. 2022, MNRAS, 511, 1647
Ginsburg, A., Sipőcz, B. M., Brasseur, C. E., et al. 2019, AJ, 157, 98
Guidry, J. A., Hermes, J. J., De, K., et al. 2024, ApJ, 972, 126
Guidry, J. A., Vanderbosch, Z. P., Hermes, J. J., et al. 2021, ApJ, 912, 125
Han, T., & Brandt, T. D. 2023, AJ, 165, 71
Harris, C. R., Millman, K. J., van der Walt, S. J., et al. 2020, Natur, 585, 357
Hawkins, K., Zeimann, G., Sneden, C., et al. 2021, ApJ, 911, 108
Hermes, J., Corcoran, K. A., Boudreaux, E. M., et al. 2018, A Method to Select Variable White Dwarfs from Gaia DR2, 21st European White Dwarf Workshop, Zenodo, doi:10.5281/zenodo.4088554
Hermes, J. J., Gänsicke, B. T., Kawaler, S. D., et al. 2017a, ApJS, 232, 23
Hermes, J. J., Kawaler, S. D., Bischoff-Kim, A., et al. 2017b, ApJ, 835, 277
Higgins, M. E., & Bell, K. J. 2023, AJ, 165, 141
Hill, G. J., Gebhardt, K., & Komatsu, E. 2008, in ASP Conf. Ser. 399, Panoramic Views of Galaxy Formation and Evolution, ed. T. Kodama, T. Yamada, & K. Aoki (San Francisco, CA: ASP), 115
Hillenbrand, L. A., Kiker, T. J., Gee, M., et al. 2022, AJ, 163, 263
Hunter, J. D. 2007, CSE, 9, 55
Ivezić, Ž., Kahn, S. M., Tyson, J. A., et al. 2019, ApJ, 873, 111
Izquierdo, P., Rodrìguez-Gil, P., Gänsicke, B. T., et al. 2018, MNRAS, 481, 703
Jenkins, J. M., Twicken, J. D., & McCauliff, S. 2016, Proc. SPIE, 9913, 99133E
Kanaan, A., Kepler, S. O., & Winget, D. E. 2002, A&A, 389, 896
Klein, B., Jura, M., Koester, D., Zuckerman, B., & Melis, C. 2010, ApJ, 709, 950
Lenz, P., & Breger, M. 2005, CoAst, 146, 53
Mainzer, A., Bauer, J., Cutri, R. M., et al. 2014, ApJ, 792, 30
Manser, C. J., Gänsicke, B. T., Eggl, S., et al. 2019, Sci, 364, 66
Manser, C. J., Gänsicke, B. T., Marsh, T. R., et al. 2016, MNRAS, 455, 4467
Masci, F. J., Laher, R. R., Rusholme, B., et al. 2019, PASP, 131, 018003
Meisner, A. M., Caselden, D., Schlafly, E. F., & Kiwy, F. 2023, AJ, 165, 36
Newville, M., Stensitzki, T., Allen, D. B., & Ingargiola, A. 2014, LMFIT: Nonlinear Least-Square Minimization and Curve-Fitting for Python, v0.8.0, Zenodo, doi:10.5281/zenodo.11813
Oke, J. B., Cohen, J. G., Carr, M., et al. 1995, PASP, 107, 375
Oke, J. B., & Gunn, J. E. 1982, PASP, 94, 586
pandas development team 2020, pandas-dev/pandas: Pandas, v2.2.3, Zenodo, doi:10.5281/zenodo.3509134
Paquette, C., Pelletier, C., Fontaine, G., & Michaud, G. 1986, ApJS, 61, 177
Perley, D. A. 2019, PASP, 131, 084503
Prochaska, J., Hennawi, J., Westfall, K., et al. 2020, JOSS, 5, 2308
Raddi, R., Gänsicke, B. T., Koester, D., et al. 2015, MNRAS, 450, 2083
Ricker, G. R., Winn, J. N., Vanderspek, R., et al. 2015, JATIS, 1, 014003
Robert, A., Farihi, J., Van Eylen, V., et al. 2024, MNRAS, 533, 1756
Rockosi, C., Stover, R., & Kibrick, R. 2010, Proc. SPIE, 7735, 77350R
Rowan, D. M., Tucker, M. A., Shappee, B. J., & Hermes, J. J. 2019, MNRAS, 486, 4574
Schröder, K. P., & Smith, R. C. 2008, MNRAS, 386, 155
Steen, M., Hermes, J. J., Guidry, J. A., et al. 2024, ApJ, 967, 166
Stellingwerf, R. F. 1978, ApJ, 224, 953
Swan, A., Farihi, J., Wilson, T. G., & Parsons, S. G. 2020, MNRAS, 496, 5233
Swan, A., Kenyon, S. J., Farihi, J., et al. 2021, MNRAS, 506, 432
Taghizadeh-Popp, M., Kim, J. W., Lemson, G., et al. 2020, A&C, 33, 100412
Thompson, S. E., & Mullally, F. 2009, JPhCS, 172, 012081
Tonry, J. L., Denneau, L., Heinze, A. N., et al. 2018, PASP, 130, 064505
Tonry, J. L., Stubbs, C. W., Lykke, K. R., et al. 2012, ApJ, 750, 99
van Sluijs, L., & Van Eylen, V. 2018, MNRAS, 474, 4603
Vanderbosch, Z. 2023, zvanderbosch/phot2lc: phot2lc v1.7.8 release, Zenodo, doi:10.5281/zenodo.8169807
Vanderbosch, Z., Hermes, J. J., Dennihy, E., et al. 2020, ApJ, 897, 171
Vanderbosch, Z. P., Rappaport, S., Guidry, J. A., et al. 2021, ApJ, 917, 41
Vanderburg, A., Johnson, J. A., Rappaport, S., et al. 2015, Natur, 526, 546
Veras, D. 2016, RSOS, 3, 150571
Virtanen, P., Gommers, R., Oliphant, T. E., et al. 2020, NatMe, 17, 261
Wilson, D. J., Hermes, J. J., & Gänsicke, B. T. 2020, ApJL, 897, L31
Xu, S., Dufour, P., Klein, B., et al. 2019, AJ, 158, 242